Available online at www.sciencedirect.com

ScienceDirect

IFAC Papers Online CONFERENCE PAPER ARCHIVE

IFAC PapersOnLine 55-37 (2022) 481–487

Experiment and Design of Prescribed-Time Safety Filter for a 7-DOF Robot Manipulator Using CBF-QP ⋆

Alexander Bertino * **Peiman Naseradinmousavi** ** **Miroslav Krstic** ***

* *Research Assistant, Dynamic Systems and Control Laboratory, Department of Mechanical Engineering, San Diego State University, San Diego, California 92115, USA (e-mail: abertino6245@sdsu.edu)*
** *Dynamic Systems and Control Laboratory, Department of Mechanical Engineering, San Diego State University, San Diego, California 92115, USA (e-mail: pnaseradinmousavi@sdsu.edu)*
*** *Department of Mechanical and Aerospace Engineering, University of California, San Diego, La Jolla, CA 92093 USA (e-mail: krstic@ucsd.edu)*

Abstract: We formulate a prescribed-time safety filter for the case of a redundant manipulator performing a fixed-duration task. This quadratic programming based formulation yields a filter that is capable of avoiding multiple obstacles in a minimally invasive manner, while simultaneously allowing the nominal controller to converge to positions located on the boundary of the safe set by the end of the fixed-duration task. In order to demonstrate the efficacy of the proposed method, we performed a series of simulations and experiments on Baxter, a 7-DOF collaborative robot manipulator. Furthermore, when compared to the exponential safety filter, which is the state-of-the-art in current literature, our proposed method yielded consistently lower joint jerks. Thus, for tasks with a fixed duration, the proposed PTSf offers performance benefits over the exponential filters currently present in literature.

Keywords: Prescribed-Time Safety Filter, Robotics, Control

1. INTRODUCTION

As the usage of robot manipulators in collaborative environments has dramatically risen in recent years, ensuring that a robot manipulator is able to operate safely has become an important goal for modern control systems (Billard and Kragic (2019)). In the past several years, a large amount of research has been devoted towards the design of control barrier functions (CBFs) for robot manipulators (Ames et al. (2019); Basso and Pettersen (2020); Chen et al. (2020); Cheng et al. (2020); Cortez and Dimarogonas (2020); Farras and Hatanaka (2021); Ferraguti et al. (2020); Hsu et al. (2015); Landi et al. (2019); Lippi and Marino (2021); Rauscher et al. (2016); Singletary et al. (2021); Wang et al. (2022); Wang and Xu (2022)). CBFs function as a safety filter for a potentially unsafe nominal controller, overriding the nominal control torques when the boundary of the safe set is approached faster than a designed convergence rate. Typically, this override torque is determined via a quadratic program minimizing the difference between the nominal and override torque, and thus CBFs can be characterized as minimally invasive. The majority of CBFs formulated for robot manipulators are based on the concept of exponential safety filters (ESfs)(Nguyen and Sreenath (2016)). Using this method, the maximum rate of convergence to the boundary of the safe set is limited to be exponential, and consequently the robot manipulator can approach but will never reach the boundary of the safe set. While ESfs are designed to be minimally invasive, their presence can interfere with the operation of set-duration tasks when the goal position of the end-effector is located near the boundary of the safe set. Under ideal conditions such as zero initial tracking error, a trajectory-tracking nominal controller operating in such a scenario would converge to the desired goal position within a fixed time that is governed by the design of the trajectory. However, when an ESf is applied to this nominal controller, the rate of approach to the goal position is limited to be exponential, and the manipulator will not reach the desired goal position by the fixed time. A considerable amount of research has been devoted towards the development of control methods for robot manipulators which are capable of guaranteeing an upper bound on the convergence time. When the nominal controller is capable of ensuring convergence within a finite-time, enforcing a condition of exponential convergence to the boundary of the safe set is counterproductive. Utilizing concepts from prescribed-time stabilization, in which convergence to the desired setpoint is achieved in a time explicitly prescribed as a controller parameter, Abel et al. (2022) have recently developed a prescribed time safety filter (PTSf) for a chain

⋆ This article is based upon work supported by the National Science Foundation under Award #1823951-1823983. The views and opinions of authors expressed herein do not necessarily state or reflect those of the United States Government or any agency thereof.

10.1016/j.ifacol.2022.11.229

of integrators. The PTSf enforces safety for a finite period of time that is explicitly set as a filter parameter T. Notably, this procedure allows the nominal controller to reach the boundary of the safe set by the end of the prescribed duration T. In order to achieve this beneficial property, a scaling of the filter gains by a function of time that grows unbounded towards the terminal time is employed. This approach can be interpreted as a safety filter that becomes less strict as the terminal time is approached, allowing the nominal controller to converge to states that are located on the boundary of the safe set. In this research effort, we reformulate the PTSf initially proposed by Abel et al. (2022) for the case of a redundant manipulator performing a fixed-duration task. This formation yields a filter that is capable of avoiding multiple obstacles in a minimally invasive manner with bounded joint torques, while simultaneously allowing the nominal controller to converge to positions located on the boundary of the safe set by the end of the fixed-duration task. In order to demonstrate the efficacy of the proposed method, we perform a series of simulations and experiments on Baxter, a 7-DOF collaborative robot manipulator. In these simulations and experiments, Baxter must follow a six second parabolic trajectory as closely as possible while navigating around a large spherical obstacle blocking its path, and place an object precisely on the surface of a table without overshoot by the end of the six seconds.

2. PRESCRIBED-TIME SAFETY FILTER FOR ROBOT MANIPULATORS

The redundant manipulator, which is being studied here, has 7-DOF. The Euler-Lagrange formulation leads to a set of 7 coupled nonlinear second-order ordinary differential equations:

$$M(q)\ddot{q} + C(q,\dot{q})\dot{q} + G(q) + F(\dot{q}) = \tau \tag{1}$$

where, $q, \dot{q}, \ddot{q} \in \mathbb{R}^7$ are angles, angular velocities and angular accelerations of joints, respectively, and $\tau \in \mathbb{R}^7$ indicates the vector of joints' driving torques. Also, $M(q) \in \mathbb{R}^{7\times7}$ is a symmetric mass-inertia matrix, $C(q,\dot{q}) \in \mathbb{R}^{7\times7}$ is a matrix of Coriolis coefficients, $G(q) \in \mathbb{R}^7$ is a vector of gravitational loading, and $F(\dot{q}) \in \mathbb{R}^7$ represents a vector of frictional torques. Our verified coupled nonlinear dynamic model of the robot (Bagheri et al. (2018); Bertino et al. (2021, 2022a)) is used as the basis of the prescribed-time safety filter approach.

We consider the following state space representation of (1):

$$\dot{Q} = \begin{bmatrix} \dot{Q}_1 \\ \dot{Q}_2 \end{bmatrix} = \begin{bmatrix} Q_2 \\ \nu(t) \end{bmatrix} \tag{2}$$

in which we define:

$$Q(t) = \begin{bmatrix} Q_1(t) \\ Q_2(t) \end{bmatrix} = \begin{bmatrix} q(t) \\ \dot{q}(t) \end{bmatrix} \tag{3}$$

$$\nu(t) = \ddot{q}(t) = M^{-1}(q)(\tau(t) - C(q,\dot{q})\dot{q}(t) - G(q) - F(\dot{q}) \tag{4}$$

The purpose of the proposed PTSF is to ensure that Baxter's end-effector remains within the following user-defined safe set for the duration of the task:

$$\mathcal{H} = \{q \in \mathbb{R}^7 | h_i(p(q)) \geq 0, \quad i = 1, ..., m\} \tag{5}$$

where

$$\frac{\partial^2 h_i}{\partial p^2} \geq 0, \quad \forall p \in \mathbb{R}^3, \quad i = 1, ..., m \tag{6}$$

and $p(q) \in R^3$ is the position of the end-effector in Cartesian coordinates, which is a function of the joint angles q. In this formulation, the robot manipulator must prevent collision between m obstacles, which each has a corresponding CBF h_i. This barrier is positive when there is no collision, 0 when the robot manipulator and the obstacle make contact, and negative when the robot manipulator is inside of the obstacle. Thus, ensuring the joint positions of Baxter are kept within the defined safe set (5) is equivalent to preventing a collision between the end-effector and an obstacle. The goal of the PTSf is formally defined as follows:

$$q(t) \in \mathcal{H} \quad \forall t \in [0, T) \tag{7}$$

where $T > 0$ is the user-defined duration of the prescribed-time task, as well as the duration of enforcement of the PTSf. In order to allow the robot manipulator to make contact with the barrier at time T, we employ a scaling of the PTSf gains by a function of time that grows unbounded towards the time T:

$$\mu_k(t) = \left(\frac{T}{T-t}\right)^k, \quad t \in [0, T), \quad k \in \mathbb{Z}_+ \tag{8}$$

Note that the temporal derivative of this function can be computed as:

$$\dot{\mu}_k(t) = \frac{k}{T}\mu_{k+1}(t), \quad t \in [0, T), \quad k \in \mathbb{Z}_+ \tag{9}$$

Due to the relative degree of the CBFs h_i being greater than 1, it is necessary to pursue a backstepping design in order to enforce the invariance of (5). To this end, we formulate the following output functions:

$$y_{i1}(t) = h_i(p(q(t))) \tag{10}$$

$$y_{i2}(t) = \frac{\partial y_{i1}(q(t))}{\partial q}\dot{q}(t) + c_1\mu_2(t)y_{i1}(t) \tag{11}$$

where $y_{i1}(t), y_{i2}(t) \in \mathbb{R}$ and $c_1 \in \mathbb{R}$ is a design parameter to be determined. In this formulation, if we ensure that y_{i1} and y_{i2} are initially positive and remain positive for the duration of the prescribed-time task, the condition (7) will also be satisfied. In order for $y_{i1}(0) > 0$, the system must initially be safe. In order for $y_{i2}(0) > 0$, we must choose:

$$c_1 > \max\left\{0, -\frac{\frac{\partial y_{i1}(0)}{\partial q}\dot{q}(0)}{y_{i1}(0)}\right\} \tag{12}$$

In order to ensure that y_{i1} and y_{i2} remain positive in the interval $t \in [0, T)$, it is necessary to examine their underlying dynamics:

$$\dot{y}_{i1} = -c_1\mu_2 y_{i1} + y_{i2} \tag{13}$$

$$\dot{y}_{i2} = \frac{2}{T}c_1\mu_3 y_{i1} + c_1\mu_2\frac{\partial y_{i1}}{\partial q}\dot{q} + \dot{q}^\top\frac{\partial^2 y_{i1}}{\partial q^2}\dot{q} + \frac{\partial y_{i1}}{\partial q}\nu \tag{14}$$

where (13) is obtained from rearranging (11), and (14) is obtained from taking the temporal derivative of (11) and applying (9). In order to enforce the positivity of h_1 and h_2 for $t \in [0, T)$, we permit only $\nu(t)$ such that the following condition is satisfied:

$$\dot{y}_{i2} + c_2\mu_2 y_{i2} \geq 0, \quad i = 1, ..., m \tag{15}$$

where $c_2 > 0$. In the next section, we will show that this is a sufficient condition for the positivity of h_i over the duration $t \in [0, T)$. Before presenting the design of the PTSf, we first reformulate (15) in terms of the CBFs h_i, as well as the joint angles q and joint velocities $\dot{q}$. To this end, we first obtain several derivatives of the CBFs with respect to the joint angles:

$$\frac{\partial h_i}{\partial q} = \frac{\partial h_i}{\partial p} J(q) \tag{16}$$

$$\dot{q}^\top \frac{\partial^2 h_i}{\partial q^2} \dot{q} = \dot{q}^\top J^\top(q) \frac{\partial^2 h_i}{\partial p^2} J(q)\dot{q} + \frac{\partial h_i}{\partial p} \dot{J}(q)\dot{q} \tag{17}$$

in which

$$J(q) = \frac{\partial p(q)}{\partial q} \tag{18}$$

where $J(q) \in \mathbb{R}^{3\times 7}$ is the jacobian of the end-effector. Then, we substitute (10), (11), (14), and (16)-(18) into (15) to obtain:

$$b_i^\top \nu \geq a_i, \quad i = 1, ..., m \tag{19}$$

where

$$a_i = -\dot{q}^\top J^\top(q) \frac{\partial^2 h_i}{\partial p^2} J(q)\dot{q} - \frac{\partial h_i}{\partial p}\dot{J}(q)\dot{q} - c_1\mu_3 \left(\frac{2}{T} + c_2\mu_1\right) h_i - (c_1 + c_2)\mu_2 \frac{\partial h_i}{\partial p} J(q)\dot{q} \tag{20}$$

$$b_i^\top = \frac{\partial h_i}{\partial p} J(q) \tag{21}$$

In order to enforce safety for the prescribed duration T in a minimally invasive manner, we apply quadratic programming minimizing the difference in joint acceleration caused by the filtered and nominal control torque:

$$\nu_{\text{safe}} = \underset{w \in \mathbb{R}^7}{\arg\min} \|w - \nu_{\text{nom}}\|^2 \tag{22}$$

$$\text{s.t.} \quad b_i^\top w \geq a_i, \quad i = 1, ..., m \tag{23}$$

where

$$\nu_{\text{nom}} = M^{-1}(q)(\tau_{\text{nom}} - C(q, \dot{q})\dot{q}(t) - G(q) - F(\dot{q})) \tag{24}$$

and τ_{nom} is the nominal control torque. The filtered control torque can then be determined as:

$$\tau_{\text{safe}} = M(q)\nu_{\text{safe}} + C(q, \dot{q})\dot{q}(t) + G(q) + F(\dot{q}) \tag{25}$$

We can now state our main result.

Theorem 1. *If $q(0) \in \mathcal{H}$, then the filtered controller (20)-(25) ensures that $q(t) \in \mathcal{H}, \forall t \in [0, T)$. Furthermore, the filtered torque τ_{safe} is uniformly bounded provided that the nominal torque τ_{nom} is continuous in t and Lipschitz in Q.*

3. PROOF OF THEOREM 1

In order to prove the invariance of the set $\mathcal{H}$ during the interval $t \in [0, T)$, it is first necessary to show that the linear inequalities (23) always have a jointly feasible solution. To this end, we construct the following feasible solution:

$$\nu_{\text{feasible}} = -(c_1 + c_2)\mu_2\dot{q} - J^+(q)\dot{J}(q)\dot{q} \tag{26}$$

where $J^+(q)$ is the Moore-Penrose pseudoinverse of $J(q)$. Substituting this expression into the condition (23) yields:

$$0 \geq -\dot{q}^\top J^\top(q) \frac{\partial^2 h_i}{\partial p^2} J(q)\dot{q} - c_1\mu_3 \left(\frac{2}{T} + c_2\mu_1\right) h_i \tag{27}$$

Utilizing the property (6), we can further simplify this inequality:

$$0 \geq -c_1\mu_3 \left(\frac{2}{T} + c_2\mu_1\right) h_i \tag{28}$$

and thus we determine that for $q(t) \in \mathcal{H}$, (23) has a jointly feasible solution. Next, we show that $q(0) \in \mathcal{H}$ ensures that $q(t) \in \mathcal{H}, \forall t \in [0, T)$. Through the application of the Comparison Lemma to (14), we obtain the following inequality:

$$y_{i2}(t) \geq y_{i2}(0) e^{c_2 T(1-\mu_1(t))} > 0, \quad \forall t \in [0, T) \tag{29}$$

Integrating (13) from 0 to t, and substituting this inequality yields:

$$y_{i1}(t) = y_{i1}(0) e^{c_1 T(1-\mu_1(t))} + \int_0^t e^{c_1 T(\mu_1(s) - \mu_1(t))} y_{i2}(s) ds > y_{i1}(0) e^{c_1 T(1-\mu_1(t))} > 0, \quad \forall t \in [0, T) \tag{30}$$

Through applying the relationship (10), we obtain:

$$h_i(t) > 0, \quad \forall t \in [0, T) \tag{31}$$

and thus $q(t) \in \mathcal{H}, \forall t \in [0, T)$.

The proof of the boundedness of the filtered torque τ_{safe} bears strong resemblance to the proof of Theorem 1 in Abel et al. (2022). Thus, in the interest of brevity, this section of the proof is not provided in this manuscript.

4. SIMULATED AND EXPERIMENTAL RESULTS

In order to assess the performance of the proposed PTSf approach, we perform both simulations using ODE methods on Baxter's dynamic equation (1), as well as experiments. In both the simulation and experiment, Baxter must track a six second trajectory designed for a pick and place task, while simultaneously avoiding collision with a large spherical obstacle blocking the trajectory, and placing its held object precisely on the surface of a table. To highlight the ability of this method to allow convergence to the barrier within a finite period of time, the nominal controller utilized in both simulations and experiments is a prescribed-time controller which we previously formulated in Bertino et al. (2022b). As we demonstrated in this earlier work, this prescribed-time nominal controller is capable of achieving zero tracking errors by the end of the six second desired trajectory. Thus, our simulations and experiments will serve to demonstrate the ability of the proposed PTSf method to allow convergence to the barrier within a finite period of time. Furthermore, we compare the performance of the PTSf method presented here to an ESf with a high gain, as well as an ESf with a low gain to highlight the strengths of the proposed method.

In the simulations and experiments, the CBF preventing collision with the spherical obstacle is formulated as:

$$h_1(p(q)) = \left\|p(q) - p_{\text{sphere}}\right\|_2^2 - R_{\text{sphere}}^2 \tag{32}$$

where $p_{\text{sphere}} \in \mathbb{R}^3$ is the position of the sphere, and $R_{\text{sphere}} \in \mathbb{R}$ is the minimum safe distance between the robot manipulator and the center of the obstacle. We formulate the CBF preventing collision with the table as:

$$h_2(p(q)) = p(q) \cdot (0, 0, 1) - z_{\text{table}} \tag{33}$$

where $z_{\text{table}} \in \mathbb{R}$ is the height of the table. For the PTSf, we set the controller parameters as $c_1 = c_2 = 1.2$. In order to prevent numerical issues arising from employing

an unbounded scaling of the gain μ_2, we clip this scaling at a maximum value $\mu_{2,\max} = 6.25$. For our six second task, this maximum is reached after 3.6 seconds of operation. For the nominal controller, we utilize the same controller parameters as in Bertino et al. (2022b), so that the interested reader can compare the performance of the PTSf + nominal controller to that of the nominal controller alone. In order to convert our formulation of a PTSf to that of an ESf, the following expression can be utilized in substitute of (20):

$$a_{i,\text{esf}} = -\dot{q}^\top J^\top(q)\frac{\partial^2 h_i}{\partial p^2}J(q)\dot{q} - \frac{\partial h_i}{\partial p}\dot{J}(q)\dot{q} \\ -2\rho^2 h_i - 3\rho\frac{\partial h_i}{\partial p}J(q)\dot{q} \tag{34}$$

with $\rho > 0$. For our high gain ESf, we set $\rho = 4$ so that the high gain ESf + nominal controller can achieve negligible tracking error at the end of the six second task. For our low gain ESf, we instead set $\rho = 1.5$ so that the low gain ESf begins to take evasive action at the same instance of time as the proposed PTSf.

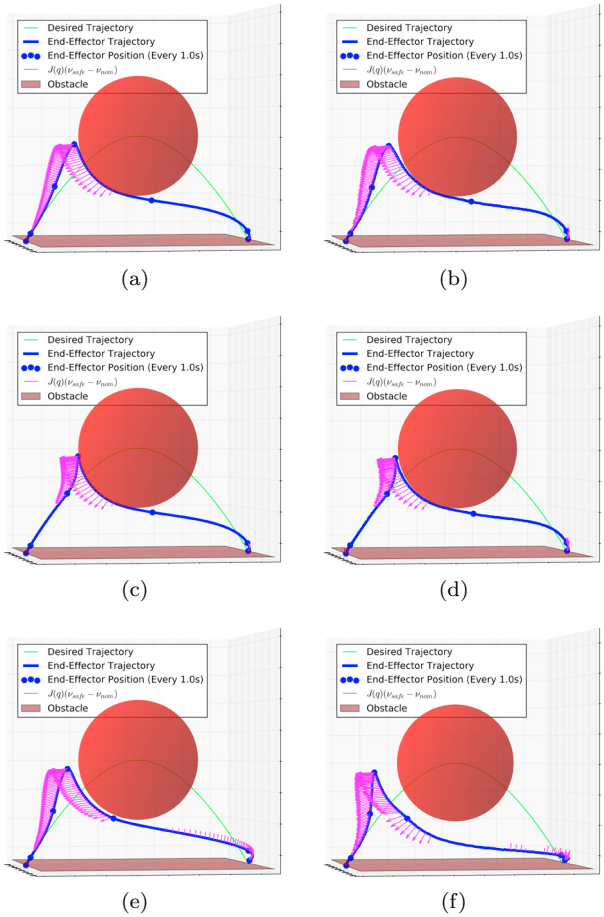

Fig. 1. Simulations (left column) and experiments (right column) of Baxter following a pick-and-place trajectory while avoiding multiple obstacles, using a prescribed-time safety filter (a, b), an exponential safety filter with a high gain of $\rho = 4$ (c, d), and an exponential safety filter with a low gain of $\rho = 1.5$ (e, f). At $t = 3s$, the end-effector trajectory takes a major turn from moving up to moving below the spherical obstacle.

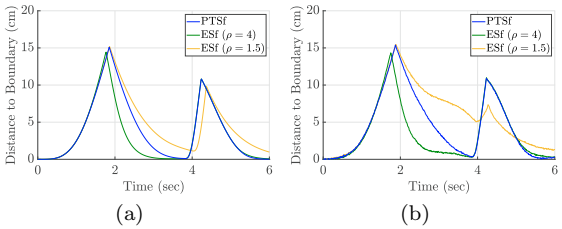

Fig. 2. The simulated (a) and experimental (b) distance between the robot manipulator and the nearest obstacle.

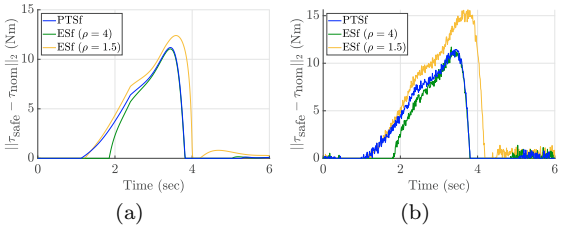

Fig. 3. The magnitude of the difference between the nominal and filtered joint torques in simulation (a) and experiment (b).

From Figure 1 it can be observed that the proposed PTSf successfully avoids the spherical obstacle in both simulation and experiment, while simultaneously placing the held object precisely on the table at the end of the six second task. Furthermore, the magnitude of the torque applied by the PTSf gradually increases as the spherical obstacle is approached, indicating that the control action is smooth and that the magnitude of the joint jerks of Baxter are not large. In comparison, the ESf with a high gain is also successful at placing the held object precisely on the table. However, the magnitude of the torque applied by the PTSf increases much more rapidly as the obstacle is approached, indicating a sharper discontinuity in the control action as well as higher joint jerks. Conversely, the ESf with a low gain appears to have joint jerks with a similar magnitude as that of the proposed PTSf, but is unable to achieve zero tracking error by the end of the six second task. Unlike both the PTSf as well as the ESf with a high gain, the ESf with a low gain becomes active towards the end of the task, limiting the rate of approach of the table to a slow exponential approach, rather than the prescribed-time approach governed by the nominal controller. The distance between the end-effector and the nearest obstacle in both simulation and experiment can be more closely observed in Figure 2. While the PTSf and high gain ESf both are able to place the held object precisely on the table, the low gain ESf instead holds the object roughly 1 cm above the table by the end of the six second task. In Figure 3, the magnitude of the difference between the nominal and filtered joint torques, can be seen. It can be observed from this figure that the PTSf and the low gain ESf both become active after around one second of operation, whereas the high gain ESf becomes active after around two seconds of operation. In order to avoid collision with the spherical obstacle while reacting at a later time, the high gain ESf ramps up in magnitude much faster than the PTSf and low gain ESf, indicating larger joint jerks during the operation of the robot manipulator at this time. After around four seconds

of operation, each safety filter rapidly drops in magnitude. This period in time corresponds with the end-effector quickly passing under the spherical obstacle, meaning that the obstacle is no longer blocking the end-effector from approaching the reference trajectory. Thus, this large change in magnitude of each safety filter is primarily due to the shape of the obstacle CBF, as well as the nominal controller rather than the convergence properties of the utilized safety filter. It is important to mention that at this instant, the safety filter with the highest experienced joint jerks is the low gain ESf. This is due to the conservative low gains of the ESf keeping the end-effector further from the reference trajectory in the beginning of the task, resulting in a larger nominal control torque to drive the system back towards the reference trajectory. During the last 2 seconds of the task, the low gain ESf maintains operation with a small magnitude, while both the high gain ESf and the PTSf do not noticably interfere with the motion of the end-effector at this time.

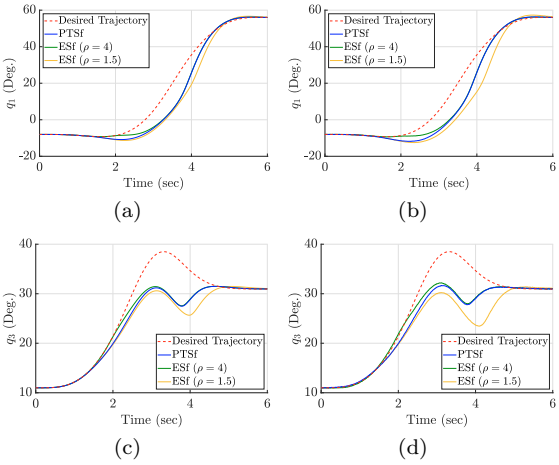

Fig. 4. The simulated (left column) and experimental (right column) joint trajectories of joints 1 and 3 of Baxter. At $t = 3s$, the end-effector trajectory takes a major turn from moving up to moving below the spherical obstacle.

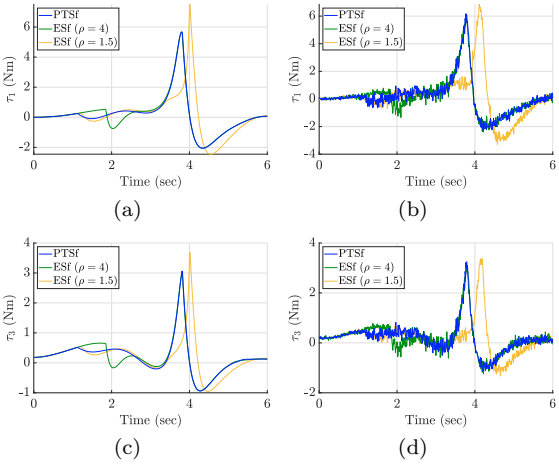

Fig. 5. The simulated (left column) and experimental (right column) joint torque input signals of joints 1 and 3 of Baxter. At $t = 3s$, the end-effector trajectory takes a major turn from moving up to moving below the spherical obstacle.

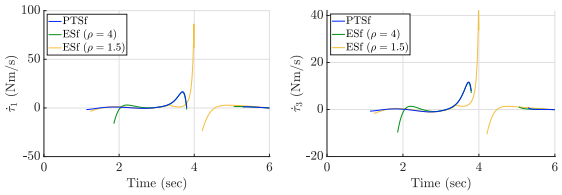

Fig. 6. The simulated joint jerks of joints 1 and 3 of Baxter, shown when the safety filter is active. At $t = 3s$, the end-effector trajectory takes a major turn from moving up to moving below the spherical obstacle.

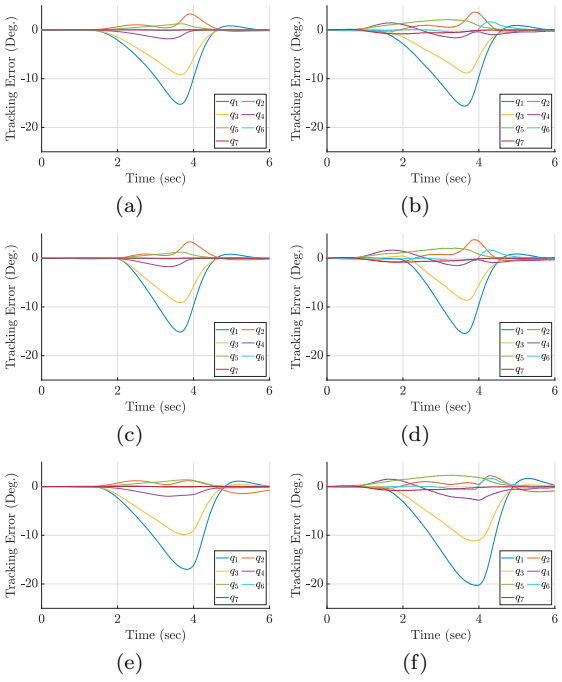

Fig. 7. Simulated (left column) and experimental (right column) tracking errors of Baxter when using a prescribed-time safety filter (a, b), an exponential safety filter with a high gain of $\rho = 4$ (c, d), and an exponential safety filter with a low gain of $\rho = 1.5$ (e, f).

The experimental, simulated, and desired joint trajectories of joints 1 and 3 of Baxter can be seen in Figure 4. In order to avoid the large spherical obstacle, joints 1 and 3 experience large deviations from the desired trajectory, with the low gain ESf experiencing the largest tracking errors. After this large deviation, the joint trajectories smoothly converge back to the desired trajectory. Observing Figure 7, it is possible to see the convergence behavior of each method in more detail. While the tracking errors for the PTSf and high gain ESf reach negligible values, there is a residual tracking error of roughly one degree on joint 2 for the low gain ESf. This joint is primarily responsible for the height of the end-effector, and thus this tracking error is present due to the low gain ESf limiting the rate of approach to the table. The experimental and simulated joint toque input signals of joints 1 and 3 of Baxter can be seen in Figure 5. It is important to note that these torques are significantly lower than the maximum torque output of Baxter's joints, which are 50 Nm for joints 1-4, and 15 Nm for joints 5-7. Thus, none of the tested methods pose

the risk of torque saturation. The simulated joint jerks of joints 1 and 3 of Baxter can be seen in Figure 6. In the beginning of the task, the joint jerk from the high gain ESf is an order of magnitude larger than either the PTSf or the low gain ESf. As the task progresses, the jerk from the high gain ESf becomes nearly identical to that of the PTSf, due to the end-effector following along the surface of the spherical obstacle. At the end of the task, both the PTSf and the high gain ESf have a negligible joint jerk compared to the low gain ESf, which actively limits the rate of approach of the end-effector to the surface of the table. Across the duration of the task, the PTSf consistently achieves the smallest joint jerks out of the tested methods, only increasing in magnitude due to the influence of the shape of the obstacle and the trajectory tracking task.

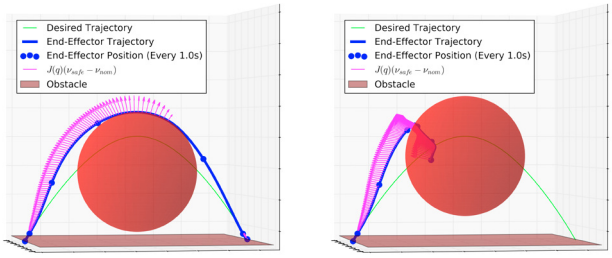

(a) (b)

Fig. 8. Simulations of Baxter following a pick-and-place trajectory while avoiding multiple obstacles, using a prescribed-time safety filter. In (a), the center of the spherical obstacle is lowered 120mm, resulting in the end-effector going over the spherical obstacle. In (b), the center of the spherical obstacle is lowered exactly 67 mm, resulting in the end-effector being unable to reach its destination. Note that in this case, the end-effector still travels along the surface of the spherical obstacle without exiting the safe set.

It is important to note that the path of the end-effector when utilizing a PTSf, as with CBF approaches in general, depends on the structure of the barrier functions h_i. For example in Figure 8(a), lowering the center of the spherical obstacle by 120mm causes the end-effector trajectory to go over the spherical obstacle rather than below it. Furthermore, as the quadratic programming filter strategy (22), (23) is a local optimization scheme, it is possible for the end-effector to get stuck on an obstacle even when there is a valid path back to the reference trajectory. In Figure 8(b), by lowering the spherical obstacle precisely 67 mm, the end-effector is no longer able to return to the reference trajectory. Even in this case however, the end-effector does not violate the safe set, and instead gently comes into contact with the spherical obstacle at the end of the six second task. The primary purpose of our proposed PTSf, as well as ESfs and other CBF based approaches is to ensure the system does not leave the safe set in a minimally invasive manner. In the context of safety, these approaches should not be seen as a substitute for path-planning, but instead as an additional layer of safety, ensuring the system remains safe even when the system does not perfectly follow the reference trajectory, or if the reference trajectory is not suitably designed to prevent collision with obstacles.

5. CONCLUSION

In this research effort, we reformulated the PTSf initially proposed by Abel et al. (2022) for the case of a redundant manipulator performing a fixed-duration task. This formation yields a filter that is capable of avoiding multiple obstacles in a minimally invasive manner with bounded joint torques, while simultaneously allowing the nominal controller to converge to positions located on the boundary of the safe set by the end of the fixed-duration task. In order to demonstrate the efficacy of the proposed method, we performed a series of simulations and experiments on Baxter, a 7-DOF collaborative robot manipulator. In these simulations and experiments, Baxter must follow a six second parabolic trajectory as closely as possible while navigating around a large spherical obstacle blocking its path, and place an object precisely on the surface of a table without overshoot by the end of the six seconds. To highlight the ability of this method to allow convergence to the barrier within a finite period of time, the nominal controller utilized in both simulation and experiment is a prescribed-time controller which we previously formulated in Bertino et al. (2022b). The results of our simulations and experiments demonstrated the ability of the PTSf to enforce safety throughout the six second task, while allowing the robot manipulator to make contact with the table and thus achieve the desired goal position by the end of the task. Furthermore, when compared to the ESf, which is the state-of-the-art in current literature, our proposed method yielded consistently lower joint jerks.

REFERENCES

Abel, I., Steeves, D., and Krstic, M. (2022). Prescribed-time safety design for a chain of integrators. *arXiv preprint arXiv:2201.09447*.

Ames, A.D., Coogan, S., Egerstedt, M., Notomista, G., Sreenath, K., and Tabuada, P. (2019). Control barrier functions: Theory and applications. In *2019 18th European control conference (ECC)*, 3420–3431. IEEE.

Bagheri, M., Krstić, M., and Naseradinmousavi, P. (2018). Multivariable extremum seeking for joint-space trajectory optimization of a high-degrees-of-freedom robot. *Journal of Dynamic Systems, Measurement, and Control*, 140(11), 111017.

Basso, E.A. and Pettersen, K.Y. (2020). Task-priority control of redundant robotic systems using control lyapunov and control barrier function based quadratic programs. *IFAC-PapersOnLine*, 53(2), 9037–9044.

Bertino, A., Naseradinmousavi, P., and Kelkar, A. (2021). Analytical and experimental decentralized adaptive control of a high-degrees-of-freedom robot manipulator. *Journal of Dynamic Systems, Measurement, and Control*, 143(7), 071007.

Bertino, A., Naseradinmousavi, P., and Krstić, M. (2022a). Delay-adaptive control of a 7-dof robot manipulator: Design and experiments. *IEEE Transactions on Control Systems Technology*.

Bertino, A., Naseradinmousavi, P., and Krstic, M. (2022b). Experimental and analytical prescribed-time trajectory tracking control of a 7-dof robot manipulator. In *2022 American Control Conference (ACC)*. IEEE.

Billard, A. and Kragic, D. (2019). Trends and challenges in robot manipulation. *Science*, 364(6446), eaat8414.

Chen, Y., Singletary, A., and Ames, A.D. (2020). Guaranteed obstacle avoidance for multi-robot operations with limited actuation: a control barrier function approach. *IEEE Control Systems Letters*, 5(1), 127–132.

Cheng, R., Khojasteh, M.J., Ames, A.D., and Burdick, J.W. (2020). Safe multi-agent interaction through robust control barrier functions with learned uncertainties. In *2020 59th IEEE Conference on Decision and Control (CDC)*, 777–783. IEEE.

Cortez, W.S. and Dimarogonas, D.V. (2020). Correct-by-design control barrier functions for euler-lagrange systems with input constraints. In *2020 American Control Conference (ACC)*, 950–955. IEEE.

Farras, A.W. and Hatanaka, T. (2021). Safe control with control barrier function for euler-lagrange systems facing position constraint. In *2021 SICE International Symposium on Control Systems (SICE ISCS)*, 28–32. IEEE.

Ferraguti, F., Bertuletti, M., Landi, C.T., Bonfè, M., Fantuzzi, C., and Secchi, C. (2020). A control barrier function approach for maximizing performance while fulfilling to iso/ts 15066 regulations. *IEEE Robotics and Automation Letters*, 5(4), 5921–5928.

Hsu, S.C., Xu, X., and Ames, A.D. (2015). Control barrier function based quadratic programs with application to bipedal robotic walking. In *2015 American Control Conference (ACC)*, 4542–4548. IEEE.

Landi, C.T., Ferraguti, F., Costi, S., Bonfè, M., and Secchi, C. (2019). Safety barrier functions for human-robot interaction with industrial manipulators. In *2019 18th European Control Conference (ECC)*, 2565–2570. IEEE.

Lippi, M. and Marino, A. (2021). A control barrier function approach to human-multi-robot safe interaction. In *2021 29th Mediterranean Conference on Control and Automation (MED)*, 604–609. IEEE.

Nguyen, Q. and Sreenath, K. (2016). Exponential control barrier functions for enforcing high relative-degree safety-critical constraints. In *2016 American Control Conference (ACC)*, 322–328. IEEE.

Rauscher, M., Kimmel, M., and Hirche, S. (2016). Constrained robot control using control barrier functions. In *2016 IEEE/RSJ International Conference on Intelligent Robots and Systems (IROS)*, 279–285. IEEE.

Singletary, A., Kolathaya, S., and Ames, A.D. (2021). Safety-critical kinematic control of robotic systems. *IEEE Control Systems Letters*, 6, 139–144.

Wang, H., Peng, J., Zhang, F., Zhang, H., and Wang, Y. (2022). High-order control barrier functions-based impedance control of a robotic manipulator with time-varying output constraints. *ISA transactions*.

Wang, Y. and Xu, X. (2022). Disturbance observer-based robust control barrier functions. *arXiv preprint arXiv:2203.12855*.